Average spin Chern number

Rafael González-Hernández [1,2,*] and Bernardo Uribe [3,†]

[1]*Departamento de Física y Geociencias, Universidad del Norte, Km. 5 Vía Antigua Puerto Colombia, Barranquilla 081007, Colombia*
[2]*Institut für Physik, Johannes Gutenberg Universität Mainz, D-55099 Mainz, Germany*
[3]*Departamento de Matemáticas y Estadística, Universidad del Norte, Km. 5 Vía Antigua Puerto Colombia, Barranquilla 081007, Colombia*

In this work we propose the average spin Chern number (ASCN) as an indicator of the topological significance of the spin degree of freedom within insulating materials. Whenever this number is a nonzero even integer, it distinguishes the material as a spin Chern insulator, and the number is a topological invariant whenever there is a symmetry that commutes with the spin and protects Chern numbers. If this number is not zero, it indicates that the material has nontrivial spin transport properties, and it lies close to the value of the spin Hall conductivity (SHC) within the band gap. For systems where the spin commutes with the Hamiltonian, the ASCN matches the SHC. When the noncommutativity of the spin with the Hamiltonian cannot be neglected, both values are nonzero simultaneously. The ASCN is therefore a good complement for the intrinsic contribution of the SHC, and permits us to detect topological information of the material, which is not possible alone from the value of the SHC.

I. INTRODUCTION

The investigation of topological phases of matter holds a central position in the landscape of condensed matter physics, tracing its origins to breakthroughs such as the quantum Hall effect and quantum spin Hall effect [1–4]. The discovery of a constant value within the band gap of the spin Hall conductivity (SHC) in topological insulators presents a compelling challenge, stimulating significant interest and inquiry [5–9]. While significant progress has been made in elucidating this issue for two-dimensional (2D) topological insulators, where the value becomes quantized in accordance with the definition of the spin Chern number (SCN), this quantization is applicable only in the nonrelativistic limit or weak spin-orbit coupling (SOC) interactions [10–15]. Nevertheless, a critical question remains unresolved, particularly concerning 3D topological insulators [16]. The constant value of the SHC within the band gap eludes a comprehensive explanation, even in the nonrelativistic limit.

The conventional approach to topological features of matter typically focuses on the exploration of electronic band structures [17,18]. However, when considering the incorporation of spin quantum degree of freedom, an additional step is required: the projection of spin operator onto the valence electronic states [19–21]. This process produces the spin spectrum, with the intrinsic topology originating from the nontrivial SCN. Using this approach, Prodan [19] defined the SCN in the thermodynamic limit, demonstrating its robustness against disorder and smooth deformations of the Hamiltonian.

Fu *et al.* [22] extended the concept to the real-space SCN for optical near fields of finite-sized structures. Recently, Lin *et al.* [20] introduced the nested spin-resolved Wilson loops and layer constructions as tools to characterize the intrinsic bulk topological properties of 3D spinful insulators, particularly focusing on identifying three distinct spin-resolved phases in helical higher-order topological insulators: 3D quantum insulators, spin-Weyl semimetals, and T-doubled axion insulator states. This spin topology classification approach provides robust topological invariants for studying the spin transport response of quantum systems [20,23].

In this study, following the definition of Prodan [19] of the spin Chern number, we introduce the concept of average spin Chern number (ASCN) as a strategic tool to unravel the nature of SHC within the band gap in 3D topological insulators. We show that the ASCN may offer valuable insights for the information underlying the SHC in insulator materials, thus indicating the interplay between spin properties and topological features in such systems. By exploring the connection between SHC and ASCN, our work aims to contribute to a deeper understanding of spin transport phenomena in 3D topological insulators. This work can be seen as a continuation of our previous efforts to understand spin properties in materials [23]. It is based on many sources, but in particular it is framed in the ideas and constructions of the colleagues working on spin-resolved topology [20].

II. PROJECTED SPIN TOPOLOGY

In an insulator, the valence states form a complex vector bundle that is known by the name of Bloch bundle. The Bloch bundle is endowed with the action of the group of crystal symmetries and moreover, it may posses time-reversal

*Contact author: rhernandezj@uninorte.edu.co
†Contact author: bjongbloed@uninorte.edu.co

symmetry, or a composition of time-reversal symmetry with a rotation, inversion or a translation in the magnetic case [24]. Incorporating spin-orbit interactions implies that the Bloch bundle is endowed with the action of the lift of the crystal symmetries to the spin group, and that time-reversal operator squares to -1.

All these symmetries endow the Bloch bundle with a rich variety of topological invariants, some of them related to magnetoelectric properties of the crystal [7,25]. Among those topological invariants we may mention the Chern-Simons axion coupling term and the Chern classes [26,27]. The first one is equivalent to the Kane-Mele invariant in the presence of time-reversal symmetry [28,29], and this invariant gives the indication of a strong topological insulating phase.

When taking into consideration the spin operator S_n in any direction n (here n is a unit vector in $\mathbb{R}^3$), we see that the Bloch bundle is moreover endowed with the action induced by this operator once it has been projected to the valence states. In other words, if P is the projection operator into the valence states

$$P := \sum_{n \in \text{occ}} |\psi_n\rangle\langle\psi_n|, \tag{1}$$

where ψ_n are the eigenstates of the Hamiltonian and occ denotes the occupied states of an insulator, the operator PS_nP defines a Hermitian operator on the Bloch bundle and its eigenvalues are between -1 and 1 (in $\hbar/2$ units) [19]. The spectrum of this projected operator will define bands whose eigenvalues are between -1 and 1, and the separation into positive and negative bands permits one to obtain topological information on the bundle.

On Hamiltonians with time-reversal symmetry the positive eigenvectors are mapped to the negative ones by the time-reversal operator, thus implying that the projected spin spectrum is symmetric with respect to zero. The projected spin operator separates the valence states into positive and the negative eigenvectors except in those points where the projected spin spectrum contains the zero. These points are localized where the positive bands of the projected spin operator cross the negative ones, and are called spin Weyl points (SWP). Their presence or absence have direct topological consequences within the material; particularly evident is the spin transport response, which we have explored in our previous work [23].

The projected spin operator may be gapped, thus separating positive from negative bands in the Bloch bundle, or it has only a finite number of SWPs in the reciprocal space. In both cases there are no SWPs in all but a finite number of k planes. Hence the Chern numbers of the positive and negative eigenstates of the projected spin operator can be determined in all but finitely many k planes.

Denoting by $\{\phi_m^+ | m \in \mathfrak{S}^+\}$ and $\{\phi_m^- | m \in \mathfrak{S}^-\}$ the positive and negative valence eigenvectors of the projected spin operator, and making a choice of oriented coordinate axes abc, the Chern numbers of the positive and negative eigenvectors on the plane $k_c = l$ with $l \in [0, 2\pi]$, can be calculated as follows:

$$c_{1,ab}^{S_n,\pm}(l) := \frac{1}{2\pi} \iint \frac{dk_a dk_b}{(2\pi)^2} \sum_{m \in \mathfrak{S}^\pm} 2\,\mathrm{Im}\left\langle \frac{\partial \phi_m^\pm}{\partial k_a} \bigg| \frac{\partial \phi_m^\pm}{\partial k_b} \right\rangle. \tag{2}$$

Since there are only a finite number of SWPs, then these Chern numbers are defined for all the planes $k_c = l$ except for a finite number of them where the SWPs lie.

The spin Chern number is thus:

$$c_{1,ab}^{S_n}(l) := c_{1,ab}^{S_n,+}(l) - c_{1,ab}^{S_n,-}(l), \tag{3}$$

and it is a well-defined integer for all but finite number of k_c planes. For systems on which the first Chern number is zero on all k planes, the spin Chern number is always twice the value of the Chern number of the positive eigenvectors. This is the case on systems with time-reversal symmetry.

Here we would like to emphasize that we are defining the spin Chern number as the difference between the Chern numbers of the positive and negative valence bands with respect to the projected spin operator. The original definition used by Kane and Mele divides this quantity by two [4]. We follow the definition of Sheng *et al.* [10] and not divide by two since we would like the spin Chern number to also take integer values on magnetic materials.

Average spin Chern number

We want to extract relevant topological information from the Bloch bundle using the whole range of spin S_n operators and all possible planes $\{xy, yz, zx\}$. So, fixing a spin direction S_n and a plane direction $ab \in \{xy, yz, zx\}$, we propose to consider the average spin Chern number (ASCN) of the projected spin operator PS_nP across all planes in reciprocal space $k_c = l$, $l \in [0, 2\pi]$:

$$\bar{c}_{1,ab}^{S_n} = \frac{1}{2\pi} \int_0^{2\pi} c_{1,ab}^{S_n}(l)\,dl. \tag{4}$$

For a set of axes with the opposite orientation bac we define the ASCN as:

$$\bar{c}_{1,ba}^{S_n} := -\bar{c}_{1,ab}^{S_n}. \tag{5}$$

We emphasize that the ASCN depends on a choice of spin direction (or spin quantization axis) and a choice of k planes on which the spin Chern numbers are calculated. Thus the ASCN should be understood as a family of quantities associated to the material. Appropriate choices of the spin direction and of the plane of integration are important in order to gain some hindsight on the spin properties of a material.

The relevance of the ASCN is based on the following properties:

(i) Whenever the spin operator commutes with the Hamiltonian, the intrinsic contribution of the SHC is a multiple of the ASCN:

$$\sigma_{ab}^c = -e\pi \cdot \bar{c}_{1,ab}^{S_c}. \tag{6}$$

Here abc is a base in a Cartesian coordinate system.

It is known that whenever the spin is a well-defined quantity, the 2D SHC is a multiple of the SCN [10,12,19,30]. In 3D materials where the Hamiltonian commutes with the spin, the SCN is a multiple of the SHC in all but a finite number of k planes. The SHC can be thus seen as the integral of the spin Chern numbers (SCNs) along parallel planes and therefore it is a multiple of the ASCN.

To make this statement precise, choose an orthogonal basis abc in the Cartesian coordinate system. Since the spin S_c and

the Hamiltonian commute, one can choose a basis of states $\psi_m^{\pm}$, which are eigenvectors of both operators:

$$H\psi_m^{\pm} = E_m^{\pm}\psi_m^{\pm} \quad \text{and} \quad S_c\psi_m^{\pm} = \pm\psi_m^{\pm}. \quad (7)$$

The SCN in the plane $k_c = l$ can be written as

$$c_{1,ab}^{S_c}(l) = \frac{1}{2\pi} \iint \frac{dk_a dk_b}{(2\pi)^2} \sum_{m \in \text{occ}} 2 \,\text{Im}\left\langle \frac{\partial(S_c\psi_m)}{\partial k_a} \middle| \frac{\partial \psi_m}{\partial k_b} \right\rangle, \quad (8)$$

where m runs over the valence states (occupied) and $S_c\psi_m = \pm\psi_m$ picks up the negative sign for the Chern number of the negative projected spin eigenvectors.

Adding the term $|\psi_r\rangle\langle\psi_r|$ running over all states (identity operator), we get the term

$$\left\langle \frac{\partial(S_c\psi_m)}{\partial k_a} \middle| \psi_r \right\rangle \left\langle \psi_r \middle| \frac{\partial \psi_m}{\partial k_b} \right\rangle. \quad (9)$$

Using the identity

$$(E_m - E_r)\langle\psi_r|\boldsymbol{\nabla}_{\mathbf{k}}\psi_m\rangle = \langle\psi_r|\boldsymbol{\nabla}_{\mathbf{k}}H|\psi_m\rangle \quad (10)$$

we see that the term of Eq. (9) becomes

$$\frac{\langle\psi_m|H_a S_c|\psi_r\rangle\langle\psi_r|H_b|\psi_m\rangle}{(E_m - E_r)^2}, \quad (11)$$

where H_a denotes $\frac{\partial H}{\partial k_a}$ and H_b denotes $\frac{\partial H}{\partial k_b}$. Replacing $H_a S_c$ by $\frac{1}{2}\{H_a, S_c\}$ and noting that $\langle\frac{\partial\psi_m}{\partial k_a}|\psi_m\rangle$ is real, we get the following formula for the SCN on the plane $k_c = l$:

$$c_{1,ab}^{S_c}(l) = \iint \frac{dk_a dk_b}{(2\pi)^3}$$
$$\times \sum_{m \in \text{occ}} \sum_{r \neq m} 2 \,\text{Im} \frac{\langle\psi_m|\frac{1}{2}\{H_a, S_c\}|\psi_r\rangle\langle\psi_r|H_b|\psi_m\rangle}{(E_m - E_r)^2}. \quad (12)$$

Further replacing the spin current operator $\hat{j}_a^c = \frac{1}{4}\{S_c, H_a\}$ and the velocity operator $\hat{v}_b = \frac{1}{\hbar}H_b$ we get:

$$-\frac{e}{2}c_{1,ab}^{S_c}(l) = \hbar \iint \frac{dk_a dk_b}{(2\pi)^3}$$
$$\times \sum_{m \in \text{occ}} \sum_{r \neq m} 2 \,\text{Im} \frac{\langle\psi_m|\hat{j}_a^c|\psi_r\rangle\langle\psi_r|-e\hat{v}_b|\psi_m\rangle}{(E_m - E_r)^2}. \quad (13)$$

The Kubo formula for the intrinsic contribution of the SHC is [31]:

$$\sigma_{ab}^c = \hbar \int dk_c \iint \frac{dk_a dk_b}{(2\pi)^3}$$
$$\times \sum_{m \in \text{occ}} \sum_{r \neq m} 2 \,\text{Im} \frac{\langle\psi_m|\hat{j}_a^c|\psi_r\rangle\langle\psi_r|-e\hat{v}_b|\psi_m\rangle}{(E_m - E_r)^2}, \quad (14)$$

and therefore we obtain the desired equality

$$\sigma_{ab}^c = \int_0^{2\pi} -\frac{e}{2}c_{1,ab}^{S_c}(l)dl = -e\pi \cdot \bar{c}_{1,ab}^{S_c}. \quad (15)$$

Here we point out that whenever the spin operator does not commute with the Hamiltonian, the 2D SHC on k planes is not a quantized quantity, as demonstrated by various authors [10,12,15,30] On the other hand, the SCN is a clearly
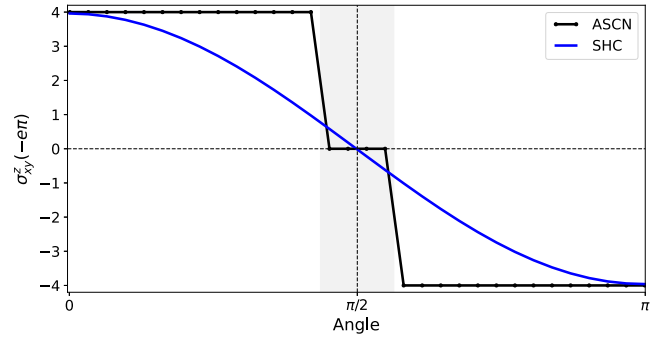
FIG. 1. SHC $n \cdot (\sigma_{xy}^x, \sigma_{xy}^y, \sigma_{xy}^z)$ (blue lines) and ASCN $\bar{c}_{1,xy}^{S_n}$ (black line with dots) for the α-BiBr material. Spin S_n is defined with $n = [\sin(\theta), 0, \cos(\theta)]$ where $0 \leqslant \theta \leqslant \pi$. The transition is presented from S_z to S_x and finishes in S_{-z}. Quantum spin Hall insulator behavior is noted in proximity to the spin directions S_z and S_{-z}. Note that there are three different phases for the ASCN, and that on each change of phase, the projected spin gap closes. On the spin directions where the ASCN is zero there is not topological contribution of the spin properties on the planes parallel to $k_x k_y$.

defined even integer number. This is the main reason we chose to define its average on the 3D Brillouin zone.

(ii) The ASCN is not linear on the spin direction n. The ASCN is not linear on the vector n defining the spin S_n, in contrast with the intrinsic contribution of the SHC, which is linear by definition. Topological invariants such as the SCN cannot vary linearly on n since its values are integers. Take for example the spin Chern number $c_{1,xy}^{S_n}(0)$ across the plane $k_z = 0$ and vary the spin S_n with $n = [\cos(\theta), 0, \sin(\theta)]$, $0 \leqslant \theta \leqslant \pi$. The spin Chern number $c_{1,xy}^{S_n}(0)$ as a function of the variable θ is a step function with even integer values, hence not linear in the spin direction.

This nonlinearity can be seen in Fig. 1 where the ASCN and the SHC have been calculated for S_n varying from S_z to S_{-z} across the planes parallel to xy in the material α-BiBr. In this material the projected spin spectrum is gapped, so the ASCN is a step function with even integer values. Also in Fig. 2(b) the ASCN and the SHC have been calculated for different values of n and for different coefficients in the 3D BHZ model. On this model, whenever the coefficient D_0 goes to zero, the location of the SWPs become less dependent on the variable θ. This is why the ASCN looks like a step function for the case $D_0 = 0.01$. The nonlinearity of the ASCN with respect to the spin direction is evident.

(iii) If the ASCN is zero in all spin directions and all reciprocal planes then there are no SWPs and all spin Chern numbers vanish. The location of the SWPs is sensitive to the direction of the spin. This can be observed in the calculation carried out in Sec. III B for the position of the SWPs for a generic spin in the 3D BHZ model presented in Sec. III. Therefore, if the ASCN is uniformly zero in all directions, it indicates the absence of SWPs. Any presence of SWPs in any spin orientation would result in a nonzero ASCN value.

Therefore, not only there are no SWPs, but also the SCNs remain constant and equal to zero. Thus the positive eigenvectors of the projected spin operator can be separated from the negative ones. The Bloch bundle is hence a sum of positive and negative bundles, and since the Chern numbers of both
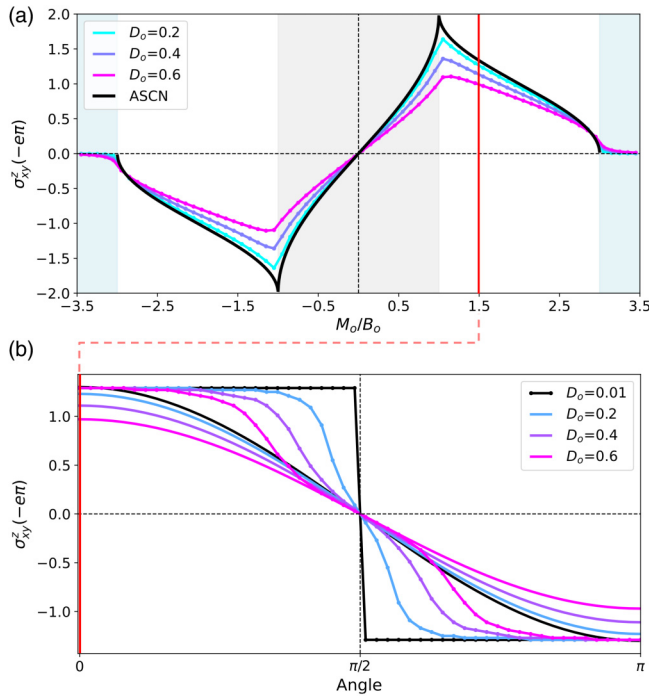
FIG. 2. Comparison of SHC with the ASCN in the 3D BHZ model using various computational and theoretical approaches. (a) Results obtained from the Kubo formula (14) of the SHC σ_{xy}^z for different values of D_0 (in colors), and the ASCN $\bar{c}_{1,xy}^{S_z}$ of (4) in reciprocal space (black line), are plotted against the $\frac{M_0}{B_0}$ parameters. The shaded areas represent different phases: the blue region denotes the trivial phase, while the white and gray areas indicate the strong and fragile phases, respectively. (b) Comparison of the SHC $n \cdot (\sigma_{xy}^x, \sigma_{xy}^y, \sigma_{xy}^z)$ (lines without dots) with the ASCN $\bar{c}_{1,xy}^{S_n}$ (lines with dots) for the spin S_n where $n = [\sin(\theta), 0, \cos(\theta)]$ and $0 \leqslant \theta \leqslant \pi$. Here we go from S_z to S_x and finish in S_{-z}. The graph (a) is at angle $\theta = 0$ and the graph (b) is at $\frac{M_0}{B_0} = 1.5$. The red vertical line in the graphs represent the same information. The strength of spin-orbit coupling (D_0) is measured in electron volts (eV).

bundles are zero across all planes, there is no contribution of the projected spin operator on the SHC. The system is trivial in terms of Chern numbers and SHC, but it may still have topological significance. The positive (and negative) bands might have nontrivial Chern-Simons θ term, potentially resulting in nontrivial surface SHC for each band group [26].

(iv) If the ASCN is an even integer for generic directions of the spin, it means that the projected spin operator has no SWPs. Therefore the material is a spin Chern insulator in the spin directions where the ASCN is nonzero. Moreover, if there is a symmetry that commutes with the spin and protects the Chern numbers, then the ASCN is a topological invariant.

Whenever time-reversal symmetry is present, the SCN is always an even integer. This follows from the fact that in the planes $k_c = 0$ the SCN is twice the value of the Chern number of the positive bands. The value of the SCN only changes by multiples of two whenever the plane is moved to $k_c = l$ and the value changes whenever SWPs are crossed.

If the ASCN is an even integer for generic directions of the spin, it means that the ASCN is constant for directions of the spin that are close to one another, and therefore there cannot

be SWPs. We show in Sec. III B that the location of the SWPs is sensitive to the direction of the spin, and since the ASCN is constant, there cannot be SWPs. If there are no SWPs for a choice of spin direction, then the SCNs are equal on parallel planes.

A spin S_n Chern insulator (SCI) is an insulator with gapped projected spin operator PS_nP whose positive bands (also negative) carry a nontrivial first Chern number [23]. The value of the ASCN parallel to $k_c = l$ planes is exactly twice the value of the Chern number of the positive bands.

Changing the direction of the spin does not close the projected spin gaps unless there is a change of topological phase for the spin operator. The change of direction of the spin might change the Chern number for the positive and negative eigenvectors of the projected spin operator, and when this happens, there is a change in the topological phase. This change of phase happens in a set of dimension 1 (curve) inside the sphere of all possible directions for the spin. Whenever there is a change of phase we claim that the ASCN changes by multiples of 4. The reasoning is the following.

In the generically gapped projected spin operator, the ASCN is a constant even number. Since ASCN is locally constant, then the SCNs are also locally constant on each plane $k_c = l$. For the ASCN to change, all the SCN must change simultaneously. This means that there must be zeros of the projected spin operator in all planes $k_c = l$ for a specific choice of spin direction S_n. These crossings must come in pairs for each plane $k_c = l$ since they appear twice on the plane $k_c = 0$ due to the time-reversal operator, and the change in SCN is the same across all parallel planes. Since on each plane, we have two crossings of the projected spin operator, the change in SCN is by multiples of 4. Hence the change of phase for the ASCN is also by multiples of 4

Whenever the ASCN is an even integer, we also might expect this number to be a topological invariant of the system. This is indeed the case if there a symmetry on the material commuting with the spin operator that moreover protects the Chern numbers on the positive and the negative bands. This is, for example, the case whenever inversion is a symmetry of the material. Inversion commutes with the spin operators, and protects the Chern numbers on the planes $k_c = 0, \pi$. But whenever there is no such symmetry commuting with the spin that protects the Chern numbers, then there is no reason to expect that the local SCNs are protected. This is the case of the SCN in 2D materials in the presence only of time-reversal symmetry. The topological invariant associated to the SCN in this case is only its value modulo 4 [19].

The even integer value of the ASCN indicates that the material has a constant SCN across all parallel k planes in a fixed spin direction. This number does not change on adiabatic deformations of the Hamiltonian if there is a symmetry that commutes with the spin, and which moreover protects Chern numbers. This particular phase is also recognized as the 3D quantum spin Hall insulator state, in analogy with the 2D [32–36].

The previous phenomena can be seen in Fig. 1 where the material α-BiBr has been studied for different directions of the spin. Here the projected spin operators are gapped, the ASCN is 4 close to S_z and -4 close to S_{-z}, while it is 0 close to

S_x. The material α-BiBr is therefore a SCI for the spin S_z but not for the spin S_x. It will have SHC for the S_z spin direction, while it for the S_x direction the SHC will be negligible. In this case the ASCN is a topological invariant of the material. This follows from the fact that inversion symmetry is present, it commutes with the spin operators, and it protects the Chern numbers on both positive and negative bands.

It is important to highlight that the material α-BiBr possesses an even more interesting topological structure. It has been found that both the positive and the negative bands possess a nontrivial Chern-Simons θ term. [20] This implies that, independently of the direction of the spin, the surface SHC is nontrivial on this material. This material α-BiBr was first recognized as a strong topological crystalline insulator [37,38], and recently has been further characterized as T-double axion insulator [20].

(v) If the Chern-Simon axion coupling term is nonzero, and the positive spin projection eigenvectors are mapped to the negative ones, then the ASCN is generically nonzero in all spin directions. In particular, the SHC is nontrivial.

Whenever the Chern-Simons coupling term is nonzero (the Kane-Mele $\mathbb{Z}_2 = 1$ invariant for time-reversal invariant systems), and the positive spin projection eigenvectors are mapped to the negative ones, then there cannot be a spin gap in any direction of the spin. If there is a spin gap, then the Bloch bundle is a sum of the positive and the negative eigenvectors, and since one is mapped to the other, the Chern-Simons coupling term of the total Bloch bundle is twice the one of the positive eigenvectors. Hence the Chern-Simons coupling term is trivial. This implies that the nontriviality of the Chern-Simons coupling term, together with a symmetry that maps positive to negative eigenvectors (such as time reversal, or a composition of time reversal with a translation), implies the nontriviality of the ASCN. The nontriviality of the ASCN implies the nontriviality of the SHC. This can be taken as one explanation of the nontriviality of the SHC on TIs [6,10].

(vi) In strong topological insulators ($\mathbb{Z}_2 = 1$) the value of the ASCN $\bar{c}_{1,ab}^{S_n}$ determines the spin Chern numbers on the planes $k_c = 0$ and $k_c = \pi$ with abc a base. If $2s < \bar{c}_{1,ab}^{S_c} < 2s + 2$ for $s \in \mathbb{Z}$ then the spin Chern numbers $c_{1,ab}^{S_n}(0)$ and $c_{1,ab}^{S_n}(\pi)$ on the planes $k_c = 0$ and $k_c = \pi$ are $2s$ and $2s + 2$ (not necessarily in this order).

In strong topological insulators there is only one pair of SWPs with opposite chirality and position. If the ASCN $c_{1,ab}^{S_n}$ lies between $2s$ and $2s + 2$ for $s \in \mathbb{Z}$, then the spin Chern numbers $c_{1,ab}^{S_n}(l)$ can only take values of $2s$ and $2s + 2$. Hence the spin Chern numbers $c_{1,ab}^{S_n}(0)$ and $c_{1,ab}^{S_n}(\pi)$ can only be $2s$ and $2s + 2$. In the STI Bi_2Te_3 the ASCN $c_{1,xy}^{S_z} = -3.16$, hence the spin Chern numbers on the planes $k_z = 0$ and $k_z = \pi$ can only be -2 and -4. The calculation shows indeed that $c_{1,xy}^{S_z}(0) = -2$ and $c_{1,xy}^{S_z}(\pi) = -4$.

The ASCN is therefore a good indicator for the existence of topological properties of the spin spectrum. It is not in general a topological invariant, in the sense that adiabatic deformations of the Hamiltonian will not leave the ASCN fixed unless the ASCN is an even integer and there is a symmetry commuting with the spin operator that protects Chern numbers.

TABLE I. Average spin Chern number ($\bar{c}_{1,ij}^z$) and spin Hall conductance (σ_{ij}^z) values for topological materials Bi_2Te_3, $MnBi_2Te_4$, and $MnBi_6Te_{10}$ and α-BiBr, where $MnBi_2Te_4$ and $MnBi_6Te_{10}$ are taken in their antiferromagnetic phase. The table includes ASCN and SHC values are given in units of $-e\pi$. The last row classifies the materials as strong topological insulator (STI), axion insulator (AI) or topological crystalline insulator [37,38] (TCI).

	Bi_2Te_3	$MnBi_2Te_4$	$MnBi_6Te_{10}$	α-BiBr
σ_{yx}^z	3.27	-2.70	-4.48	-3.96
$\bar{c}_{1,xy}^{S_z}$	3.16	-2.60	-5.04	-4
σ_{xy}^z	-3.25	2.70	4.48	3.66
Type	STI	AI	AI	TCI

When the ASCN is nonzero, it implies a corresponding nonzero value for the SHC, and the intensity of the SHC is linked to the magnitude of the ASCN. In Table I we have collected the values of the ASCN and the SHC for different materials with topological properties. It is important to note that their values are related, and moreover, that we can deduce from the value of the ASCN the fact that α-BiBr has a projected spin gap and therefore it is a spin Chern insulator. Additionally, we deduce that the spin Chern numbers for $MnBi_6Te_{10}$ are -6 and -4 on the $k_z = 0$ and $k_z = \pi$ planes, respectively.

The ASCN can also be calculated in Weyl semimetals. The occupied states restricted to a plane $k_c = l$ are gapped except where the energy meets the Fermi energy, which happens only at a finite number of k points. Moreover, the projected spin operator is always gapped for the planes $k_c = l$ except for a finite number of planes. Hence the SCN is well defined for all planes $k_c = l$, except for a finite number of planes where Weyl points are located. In the case of Weyl semimetals, the value of the ASCN will be very close to the one of the SHC since the eigenvalues of the projected spin operator will be close to 1 and -1 [39].

Note that the average Chern number (ACN) can also be define on the occupied states:

$$\bar{c}_{1,ab} = \frac{1}{2\pi} \int_0^{2\pi} c_{1,ab}(l)dl. \tag{16}$$

Here $c_{1,ab}(l)$ is the first Chern number of the occupied states restricted to the plane $k_c = l$. In this case it follows that the AHC is a multiple to the ACN, no matter what the Fermi energy level is. In formulas we have

$$\sigma_{ab} = \frac{e^2}{h} 2\pi \cdot \bar{c}_{1,ab}. \tag{17}$$

So we can interpret the AHC as the average contribution of the Chern numbers across parallel planes in reciprocal space. This number is therefore directly linked with the distance in momentum space of the Weyl points in Weyl semimetals [40,41].

III. 3D BHZ MODEL

We have carried out extensive calculations for the ASCN and its relation to the SHC in the 3D BHZ model of four

bands [5]. The BHZ Hamiltonian can be written as:

$$H(\mathbf{k}) = M(\mathbf{k})\tau_3\sigma_0 + A(\mathbf{k})\tau_1\sigma_3 + C(\mathbf{k})\tau_2\sigma_0 + D(\mathbf{k})\tau_1\sigma_1,$$
(18)

with

$$M(\mathbf{k}) = M_0 - B_0[\cos(k_x) + \cos(k_y) + \cos(k_z)],$$
(19)

$$A(\mathbf{k}) = A_0 \sin(k_x),$$
(20)

$$C(\mathbf{k}) = C_0 \sin(k_y),$$
(21)

$$D(\mathbf{k}) = D_0 \sin(k_z),$$
(22)

spin matrices $S_x = \tau_0\sigma_1$, $S_y = \tau_3\sigma_2$ and $S_z = \tau_0\sigma_3$, time reversal $\mathbb{T} = i\tau_0\sigma_2\mathbb{K}$ where $\mathbb{K}$ is complex conjugation, and inversion $I = \tau_0\sigma_3$ [23].

Whenever $D_0 = 0$ we have the original 2D BHZ Hamiltonian consisting of two disconnected blocks related by time-reversal symmetry. In this context, the nontrivial off-diagonal term D could be interpreted as the spin-orbit coupling term in the 3D layered system. This new term also breaks the commutativity with the spin operator.

In matrix form the Hamiltonian is

$$H(\mathbf{k}) = \begin{pmatrix} M & A+iC & 0 & D \\ (A+iC)^* & -M & D & 0 \\ 0 & D & M & -(A+iC)^* \\ D & 0 & -(A+iC) & -M \end{pmatrix},$$
(23)

it preserves time-reversal symmetry and inversion since the function $M(\mathbf{k})$ is even and the functions $A(\mathbf{k}), C(\mathbf{k}), D(\mathbf{k})$ are odd with respect to inverting $\mathbf{k}$.

The energy of the Hamiltonian is degenerate with $E = \pm\lambda$, and

$$\lambda = \sqrt{(M^2 + A^2 + C^2 + D^2)}.$$
(24)

One choice of eigenvectors of the Hamiltonian is

$$v_1 := (M - \lambda, A - iC, 0, D)^T$$
(25)

$$v_2 := (A + iC, -M - \lambda, D, 0)^T$$
(26)

$$v_3 := (M + \lambda, A - iC, 0, D)^T$$
(27)

$$v_4 := [-(A + iC), M - \lambda, -D, 0]^T$$
(28)

with v_1 and v_2 with energy $-\lambda$ and v_3 and v_4 with energy λ. The energy of the spectrum is gapless whenever $M = A = C = D = 0$ and this happens only whenever $\frac{M_0}{B_0} = -3, -1, 1, 3$. Otherwise the energy has a gap.

Furthermore note that $\mathbb{T}I$ preserves the energies and the $\mathbf{k}$ points. Therefore $\mathbb{T}Iv_1$ is also an eigenvector of the Hamiltonian and it is spanned by v_1 and v_2. In the base given above one can calculate explicitly the coefficients of both $\mathbb{T}Iv_1$ and $\mathbb{T}Iv_2$ with respect to v_1 and v_2.

More important is the spin operator and its projected version. Consider the projected version PS_nP of the spin operator S_n where P is the projection into the occupied states and n is

a generic direction. In the BHZ model we have

$$P = |\psi_1\rangle\langle\psi_1| + |\psi_2\rangle\langle\psi_2|,$$
(29)

where the normalized base is

$$\psi_i = \frac{1}{|v_i|}v_i.$$
(30)

The projected spin operator acts on the vector spaces of occupied states and returns a linear combination of occupied states. The spectrum of the projected spin operator in the reciprocal space will be denoted spin spectrum, and it splits into two main cases. Either the spin spectrum is gapped or not.

In the BHZ Hamiltonian the spin spectrum is not gapped whenever $-3 < \frac{M_0}{B_0} < 3$, and since the energies are always degenerate, the spin spectrum crosses the 0 line in points. These points are called spin Weyl points (SWP) [23].

A. ASCN for S_z

Focusing at the projected S_z spectrum, we know that the SWPs are located at the points [23]:

$$\left[0, 0, \arccos\left(\frac{M_0}{B_0} + 2\right)\right] \quad \text{for} \quad -3 < \frac{M_0}{B_0} < -1 \quad (31)$$

$$\left.\begin{array}{l} \left[0, \pi, \arccos\left(\frac{M_0}{B_0}\right)\right] \\ \left[\pi, 0, \arccos\left(\frac{M_0}{B_0}\right)\right] \end{array}\right\} \quad \text{for} \quad -1 < \frac{M_0}{B_0} < 1 \quad (32)$$

$$\left[\pi, \pi, \arccos\left(\frac{M_0}{B_0} - 2\right)\right] \quad \text{for} \quad 1 < \frac{M_0}{B_0} < 3. \quad (33)$$

Denote by $\mathbf{k}_0$ any of these points. Note that on these points, the projection on the valence bands of the S_z operator applied of the valence eigenstates is precisely zero. What this means theoretically is that on $\mathbf{k}_0$

$$S_z\psi_1(\mathbf{k}_0)\rangle = \sum_{j=3,4} |\psi_j(\mathbf{k}_0)\rangle\langle\psi_j(\mathbf{k}_0)|\widehat{S}_z\psi_1(\mathbf{k}_0)\rangle \quad (34)$$

and therefore the S_z of the valence bands on the point $\mathbf{k}_0$ is all conduction (see Fig. 3). This means that the 3D BHZ models an insulator for the Hamiltonian but not for the projected spin.

Around the SWP we could put a small 2D sphere surrounding it. On this sphere the S_z operator splits into valence and conduction part. The way the negative projected spin spectrum eigenvectors twirl around the spin Weyl point is measured by the chirality of the point (Chern number). The SWPs are topologically protected whenever their chiralities are different from zero. Their positions may vary through adiabatic perturbations of the Hamiltonian, but their chiralities will remain fixed.

The values of the SCN for the projected spin S_z operator on the planes $k_j = 0, \pi$ for $j = x, y, z$ permits us to determine the ASCN on the three cases. That is:

$$\overline{c}_{1,xy}^{S_z} = \begin{cases} -2 + \frac{2}{\pi}\arccos\left(\frac{M_0}{B_0} + 2\right) & \text{for} \quad -3 < \frac{M_0}{B_0} < -1 \\ 2 - \frac{4}{\pi}\arccos\left(\frac{M_0}{B_0}\right) & \text{for} \quad -1 < \frac{M_0}{B_0} < 1 \\ \frac{2}{\pi}\arccos\left(\frac{M_0}{B_0} - 2\right) & \text{for} \quad 1 < \frac{M_0}{B_0} < 3 \end{cases}$$
(35)
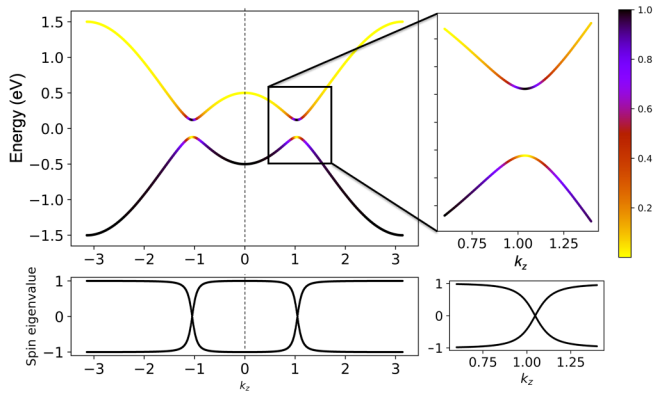
FIG. 3. Graph of the projection of the positive projected spin S_z eigenvector into the valence and conduction bands on the 3D BHZ model at the k_z axis on the point $(k_x, k_y) = (0, \pi)$ for $\frac{M_0}{B_0} = 0.5$, $A_0 = C_0 = 1, D_0 = 0.11$. The SWPs are located on this axis and the graph of the projected spin eigenvalues lies at the bottom. The top graphs are the degenerate energies of the four bands, and the color represents the square of the norm of the projection of the positive spin eigenvector of PS_zP into the valence and the conduction states respectively. If ϕ is the positive eigenvector of PS_zP, then the color on the upper bands represent the value $|\langle\psi_3|\phi\rangle|^2 + |\langle\psi_4|\phi\rangle|^2$ and on the bottom bands the value $|\langle\psi_1|\phi\rangle|^2 + |\langle\psi_2|\phi\rangle|^2$. In the location of the SWPs, the spin S_z of both the valence states ψ_1 and ψ_2, is all conduction. Even though the 3D BHZ model has an energy gap, at some points in momentum space the spin of the valence states lies on the conduction band. The BHZ models an energy insulator, which does not insulate the spin.

These results are highlighted by the red line depicted in Fig. 2. Here it is important to notice that noninteger values of the ASCN implies the existence of SWPs.

The SOC could be interpreted as the matrix $D\tau_1\sigma_1$ and its intensity as the value of D_0. In Fig. 2(a) the ASCN $\bar{c}^{S_z}_{1,xy}$ has been plotted with respect to the value of $\frac{M_0}{B_0}$, together with the SHC σ^z_{xy} for different values of D_0.

It is important to note that the ASCN remains unaffected by the value of D_0, serving as a direct measure of the SWP's distance. Notably, in the case of $D_0 = 0$, the ASCN aligns with the SHC and the intensity of the SHC decreases for bigger D_0; however, both the ASCN and the SHC retain nonzero values simultaneously.

B. SWP for generic spin

Consider the unitary vector $n = (\alpha, \beta, \gamma)$ and the generic spin $S_n = n \cdot (S_x, S_y, S_z)$. If ψ_j are the eigenvectors of the Hamiltonian forming a unitary base (norm one and perpendicular to one another), then the projected spin matrix is defined as follows:

$$(M_{S_n})_{ij} = \langle\psi_i|S_n|\psi_j\rangle \quad i, j \in \{1, 2\}. \tag{36}$$

The projected spin eigenvalues vanish whenever the whole projected spin matrix vanishes. Note that in this case we could use the degenerate basis $\{v_1, v_2\}$ of Eqs. (25) and (26) in order to solve the equations

$$\langle v_i|S_n|v_j\rangle = 0 \quad i, j \in \{1, 2\}. \tag{37}$$

Let us calculate first the matrix elements $\langle v_i|S_{x_k}|v_j\rangle$ for $k = 1, 2, 3$:

$$\langle v_1|S_x|v_1\rangle = 2DA \tag{38}$$

$$\langle v_1|S_x|v_2\rangle = -2\lambda D \tag{39}$$

$$\langle v_2|S_x|v_1\rangle = -2\lambda D \tag{40}$$

$$\langle v_2|S_x|v_2\rangle = 2DA \tag{41}$$

$$\langle v_1|S_y|v_1\rangle = -2DC \tag{42}$$

$$\langle v_1|S_y|v_2\rangle = 2i\lambda D \tag{43}$$

$$\langle v_2|S_y|v_1\rangle = -2i\lambda D \tag{44}$$

$$\langle v_2|S_y|v_2\rangle = -2DC \tag{45}$$

$$\langle v_1|S_z|v_1\rangle = (M - \lambda)^2 + A^2 + C^2 - D^2 \tag{46}$$

$$\langle v_1|S_z|v_2\rangle = 2(A + iC)\lambda \tag{47}$$

$$\langle v_2|S_z|v_1\rangle = 2(A - iC)\lambda \tag{48}$$

$$\langle v_2|S_z|v_2\rangle = (M + \lambda)^2 + A^2 + C^2 - D^2. \tag{49}$$

The projected spin matrix has for entries:

$$(M_{S_n})_{11} = 2\alpha DA - 2\beta DC + \gamma((M - \lambda)^2 + A^2 + C^2 - D^2) \tag{50}$$

$$(M_{S_n})_{21} = -2\alpha\lambda D + 2i\beta\lambda D + 2\gamma\lambda(A + iC) \tag{51}$$

$$(M_{S_n})_{12} = -2\alpha\lambda D - 2i\beta\lambda D + 2\gamma\lambda(A - iC) \tag{52}$$

$$(M_{S_n})_{22} = 2\alpha DA - 2\beta DC + \gamma((M + \lambda)^2 + A^2 + C^2 - D^2). \tag{53}$$

The projected spin matrix has zero eigenvalues whenever all entries are zero. Subtracting $(M_{S_n})_{11} = 0$ from $(M_{S_n})_{22} = 0$ we see that $M = 0$, and therefore

$$\alpha DA - \beta DC + 2\gamma(A^2 + C^2) = 0. \tag{54}$$

From $(M_{S_n})_{21} = 0$ we see that

$$\alpha D - i\beta D + \gamma(A + iC) = 0. \tag{55}$$

Replacing $A + iC = \frac{-\alpha + i\beta}{\gamma}D$ in Eq. (54) we see that the equation is satisfied. Then we only need to consider the equations $M = 0$ and $\alpha D - i\beta D + \gamma(A + iC) = 0$. These equations can be written as:

$$\cos(k_x) + \cos(k_y) + \cos(k_z) = \frac{M_0}{B_0} \tag{56}$$

$$\gamma A_0 \sin(k_x) + \alpha D_0 \sin(k_z) = 0 \tag{57}$$

$$\gamma C_0 \sin(k_y) - \beta D_0 \sin(k_z) = 0. \tag{58}$$

Let us see some explicit choices of n. $n = (0, 0, 1)$, in this case we have that $k_x, k_y = 0, \pi$ and $k_z = \arccos(\frac{M_0}{B_0} + \{2, 0, -2\})$ depending on the location of $\frac{M_0}{B_0}$. $n = (1, 0, 0)$, $n = (0, 1, 0)$ or any combination of the two. In this case the

system is degenerate and the matrix is zero on the whole $k_z =| 0$ plane. $n = (\frac{1}{\sqrt{2}}, 0, \frac{1}{\sqrt{2}})$, and moreover $A_0 = C_0 = D_0$, then we have that $k_y = 0, \pi$, $k_x = -k_z$, and $2\cos(k_x) = \frac{M_0}{B_0} \pm 1$.

In general, for any direction n of the spin, there is a pair of opposite chiralities SWPs in the Bulk whenever $1 < |\frac{M_0}{B_0}| < 3$. For $|\frac{M_0}{B_0}| < 1$ there are two pairs of opposite chiralities SWPs. Their location is defined by the solution of the equations defined above.

In Fig. 2(b) we have plotted the ASCN $\overline{c}_{1,xy}^{S_n}$ and the SHC for values of $n = [\sin(\theta), 0, \cos(\theta)]$ where $0 \leqslant \theta \leqslant \pi$. The ASCN only depends on the location and chiralities of the SWPs for each choice of n, while the SHC can be calculated by the expression

$$\sigma_{xy}^n = \sin(\theta)\sigma_{xy}^x + \cos(\theta)\sigma_{xy}^z. \tag{59}$$

In Fig. 2(b) it is observed that the SHC exhibits alignment with the ASCN when the spin direction rotates along the k_y axis. In this graph, it is noted that both ASCN and SHC undergo a change in sign from S_z (angle $= 0$) to S_{-z} (angle $= \pi$).

In Fig. 3 we have plotted the energy bands on the k_z axis for $(k_x, k_y) = (0, \pi)$ for specific choice of constants. The SWPs are located on this axis. We have colored the energy bands with the square of the norm of the projection of $S_z|\phi\rangle$ on the valence and the conduction bands where ϕ is the eigenvector of the projected spin operator PS_zP with smallest positive eigenvalue. Note that at the SWPs, the spin of the valence energy states is all conduction. Namely, even though the BHZ models an insulator in terms of its energy spectrum, it is not an insulator on the spin spectrum.

IV. MATERIALS

In order to demonstrate the applicability of the current methodology to real-world materials, we have calculated the ASCN and SHC for different insulator materials. Here we contrast the results for the case of Bi_2Te_3, $MnBi_2Te_4$, $MnBi_6Te_{10}$, and α-BiBr, which were chosen due to their predicted topological properties [18,20,37,38,42,43]. Previous works classified them as either strong topological insulators, axion insulators, or quantum Hall spin insulators. The structural parameters for these materials were obtained from the Materials Project [44] and previous studies [43].

The calculations were performed using a combination of first-principles methods based on the VASP [45], the WANNIER90 [46], and the PYTHTB code [47], with detailed computational setups outlined in our previous work [23]. However, computational tools have recently been created to study the spin topology of materials [20,48].

We evaluated the electronic and spin spectra of these materials, including the projection of spin projected eigenvalues (PS_zP) onto the electronic bands, as depicted in Fig. 4. For the case of Bi_2Te_3, we observed a pronounced concentration of valence spin information around a singular point in the conduction band along the ΓT k path. This localization of spin information suggests the existence of a spin Weyl point along the ΓT path, as depicted in Fig. 4(a). Remarkably, the projected spin spectrum calculation unveils the presence of spin

Weyl points both in the TΓ and $-$TΓ paths, which represent the diagonal direction in the rhombohedral phase or z axis in Cartesian coordinates. Consequently, the ASCN is expected to be proportional to the distance between these SWPs, as in the 3D BHZ model. Indeed, we have found that the both ASCN and SHC exhibit a proportional relationship with the SWPs distance. Table I presents the value of ASCN and SHC for Bi_2Te_3, demonstrating a topological response across all k_z planes in the hexagonal BZ. Notably, the SHC signal is particularly pronounced along the z axis, coinciding with the location of SWP in reciprocal space. This result aligns with the layered structure of Bi_2Te_3, where the z planes correspond to the layers in real space [49].

We have performed an analysis of the electronic and projected spin spectrum of α-BiBr, uncovering a nonzero energy and projected spin gap throughout the entire Brillouin zone. This characteristic serves to classify the α-BiBr as both as a material with both energy gap and spin gap, as it shown in Fig. 4(b), in agreement with Lin *et al* [20]. Furthermore, no significant exchange of spin information between the conduction and valence bands is evident. However, we have observed a constant $\overline{c}_{1,xy}^z$ value of -4 along all the k_z planes and zero of the k_x and k_y planes in the Brillouin zone for α-BiBr, which is consistent with the $\sigma_{yx}^z \sim -4$ as presented in Table I. The alignment between SHC and ASCN reflects the full topological response of α-BiBr perpendicular to the z axis. This result is hidden for the $\mathbb{Z}_2 = 0$ index for this material, highlighting the efficacy of ASCN as a tool for extracting valuable insights into the spin response of topological insulators. Here it is worth mentioning that each group of bands, the positive and the negative, possess nontrivial Chern-Simons θ term [20]. This implies that independent of the spin direction, it will give rise to a surface SHC contribution in a finite sample.

It is found that α-BiBr displays a vanishing ASCN for the S_x and S_y spin components, suggesting a lack of topological response in SHC for these spin directions. Our calculations confirm α-BiBr as a 3D quantum spin Hall insulator (S_z). The observed anisotropy between σ_{xy}^z and σ_{yx}^z responses is further supported by symmetry analysis of the SHC tensor, indicating distinct components within this space group (#12). This convergence of ASCN and SHC values highlights the unique topological nature of α-BiBr.

Regarding the axion insulators (AI) $MnBi_2Te_4$ and $MnBi_6Te_{10}$, we also see that the values of the ASCN and SHC are very similar. In these two materials time-reversal coupled with a translation is a preserved symmetry, and therefore the Chern numbers of the positive and negative projected spin eigenvectors are inverse to one another. Therefore we can conclude that the spin Chern number on all k_z planes for $MnBi_2Te_4$ are less than -2 and for $MnBi_4Te_{10}$ are less than -4. These findings align with the nontrivial results of the pseudo SCN for the $MnBi_2Te_4$ family, as obtained by Wang *et al.* [50].

With the SHC alone we may not distinguish the materials in Table I, but with the incorporation of the ASCN we differentiate α-BiBr from the others. The incorporation of the ASCN into the set of material classifiers will help distinguish QSHIs from strong topological and axion insulators, and moreover, it will permit us to distinguish the topological features underlying the projected spin operator.
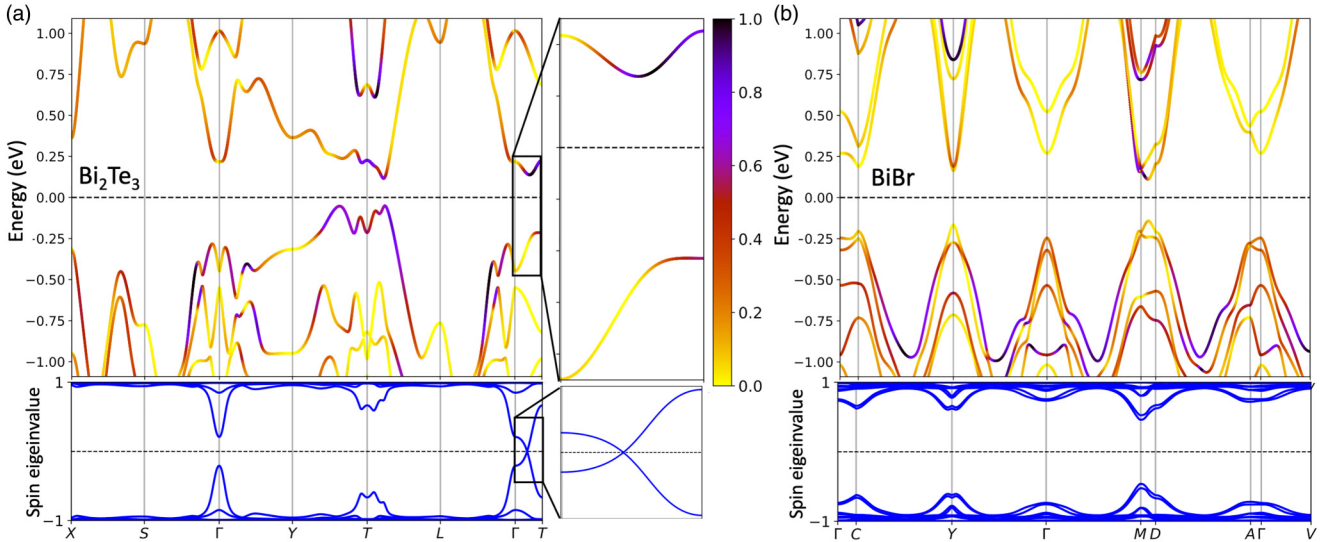
FIG. 4. Energy bands and projected spin S_z eigenvalues for the strong topological insulator Bi_2Te_3 and the weak topological insulator α-BiBr. The color on the energy bands represent the square of the norm of the projection of the smallest positive projected spin eigenvector into each pair of degenerate bands, both valence and conduction. If ϕ is the eigenvector of the smallest positive eigenvalue of PS_zP, the color on each pair of consecutive degenerate bands ψ_{2n-1}, ψ_{2n} is given by the value $|\langle\psi_{2n-1}|S_z\phi\rangle|^2 + |\langle\psi_{2n}|S_z\phi\rangle|^2$. (a) Bi_2Te_3 is a strong topological insulator, and as such, it has SWPs on the T-Γ-T path. The chiralities of these SWPs is ± 1 and the ASCN is $c_{1,xy}^{S_z} = 3.16$, which means that the SWPs are located almost in the middle of the T-Γ path. Note that the value of the intrinsic SHC is $\sigma_{yx}^z = 3.27$, which is very close to the ASCN. The eigenvector of the projected spin operator with smallest positive eigenvalue is entirely conduction on the SWPs. This can be seen in the Γ-T path. (b) α-BiBr is a spin Chern insulator since the value of the ASCN $c_{1,xy}^{S_z} = -4$ is a nonzero even integer. The spin insulation can be read from the fact that the ASCN is an even integer, and the topological feature is given by the constant value of -4 for the SCN on the k_xk_y planes. Since this SCN is a multiple of 4, the Chern number of the positive and negative projected spin eigenvectors is equal to 2 and -2, respectively. Hence the number of pairs of negative eigenvalues of the inversion operator is even and therefore the strong topological insulator marker $\mathbb{Z}_2$ of Fu-Kane-Mele is equal to zero. Nevertheless, it has been shown [20] that the Chern-Simons axion θ term of both the positive and the negative bands is nontrivial. Thus, independent of the spin direction, the surface SHC contribution is nontrivial. This material α-BiBr was firstly recognized as a strong topological crystalline insulator [37,38], and recently has been characterized also as a $\mathbb{T}$-double axion insulator [20].

It is also important to remark that the ASCN calculations are significantly less intensive compared to SHC calculations. The former needs 3D dense k grids while the latter only needs a dense k grid in one dimension. The ASCN can also be calculated in collinear ferromagnetic or antiferromagnetic when the spin z component can be consider a good quantum number in the weak SOC limit. These results indicate the practical advantage of employing ASCN as a computational tool and topological indicator, in scenarios where the efficient calculation of SHC is limited.

protects Chern numbers, the value of the ASCN is a topological invariant.

From a computational perspective, calculating the ASCN is less computationally intensive compared to the SHC. For the latter, a 3D dense grid is mandatory, while for the former just a dense grid in the direction of integration is necessary. The calculation of the Chern numbers does not require dense grids. Understanding the ASCN for various spin directions and planes contributes to the comprehension and categorization of insulating materials, enhancing our knowledge of their topological properties and aiding in their classification.

V. CONCLUSION

The ASCN consists of a family of numbers associated with a choice of spin direction and a choice of plane of integration. These numbers provide hindsight of the spin properties of an insulator material. If the ASCN is nonzero for a specific choice of spin direction, then a signal in the SHC should be expected. Moreover, if the material is an STI, then the ASCN is different from zero. Therefore, materials with nonzero values for the ASCN include all STIs. When the ASCN is an even integer, then there is a gap in the projected spin operator, and therefore the Kane-Mele invariant $\mathbb{Z}_2$ is trivial. Moreover, if there is a symmetry commuting with the spin, which

[1] D. J. Thouless, M. Kohmoto, M. P. Nightingale, and M. den Nijs, Quantized Hall conductance in a two-dimensional periodic potential, Phys. Rev. Lett. **49**, 405 (1982).

[2] F. D. M. Haldane, Model for a quantum Hall effect without landau levels: Condensed-matter realization of the "parity anomaly", Phys. Rev. Lett. **61**, 2015 (1988).

[3] J. Sinova, S. O. Valenzuela, J. Wunderlich, C. H. Back, and T. Jungwirth, Spin Hall effects, Rev. Mod. Phys. **87**, 1213 (2015).

[4] C. L. Kane and E. J. Mele, Quantum spin Hall effect in graphene, Phys. Rev. Lett. **95**, 226801 (2005).

[5] B. A. Bernevig, T. L. Hughes, and S.-C. Zhang, Quantum spin Hall effect and topological phase transition in HgTe quantum wells, Science **314**, 1757 (2006).

[6] T. Fukui and Y. Hatsugai, Topological aspects of the quantum spin-Hall effect in graphene: Z_2 topological order and spin Chern number, Phys. Rev. B **75**, 121403(R) (2007).

[7] X.-L. Qi, T. L. Hughes, and S.-C. Zhang, Topological field theory of time-reversal invariant insulators, Phys. Rev. B **78**, 195424 (2008).

[8] M. Z. Hasan and C. L. Kane, *Colloquium*: Topological insulators, Rev. Mod. Phys. **82**, 3045 (2010).

[9] X.-L. Qi and S.-C. Zhang, Topological insulators and superconductors, Rev. Mod. Phys. **83**, 1057 (2011).

[10] D. N. Sheng, Z. Y. Weng, L. Sheng, and F. D. M. Haldane, Quantum spin-Hall effect and topologically invariant chern numbers, Phys. Rev. Lett. **97**, 036808 (2006).

[11] R. Chen and B. Zhou, Spin Chern number and topological phase transition on the Lieb lattice with spin–orbit coupling, Phys. Lett. A **381**, 944 (2017).

[12] F. Matusalem, M. Marques, L. K. Teles, L. Matthes, J. Furthmüller, and F. Bechstedt, Quantization of spin Hall conductivity in two-dimensional topological insulators versus symmetry and spin-orbit interaction, Phys. Rev. B **100**, 245430 (2019).

[13] M. Ezawa, Symmetry protected topological charge in symmetry broken phase: Spin-Chern, spin-valley-Chern and mirror-Chern numbers, Phys. Lett. A **378**, 1180 (2014).

[14] Q.-X. Lv, Y.-X. Du, Z.-T. Liang, H.-Z. Liu, J.-H. Liang, L.-Q. Chen, L.-M. Zhou, S.-C. Zhang, D.-W. Zhang, B.-Q. Ai, H. Yan, and S.-L. Zhu, Measurement of spin Chern numbers in quantum simulated topological insulators, Phys. Rev. Lett. **127**, 136802 (2021).

[15] R. Favata and A. Marrazzo, Single-point spin chern number in a supercell framework, Electron. Struct. **5**, 014005 (2023).

[16] S. M. Farzaneh and S. Rakheja, Intrinsic spin Hall effect in topological insulators: A first-principles study, Phys. Rev. Mater. **4**, 114202 (2020).

[17] M. G. Vergniory, B. J. Wieder, L. Elcoro, S. S. P. Parkin, C. Felser, B. A. Bernevig, and N. Regnault, All topological bands of all nonmagnetic stoichiometric materials, Science **376**, eabg9094 (2022).

[18] B. Bradlyn, L. Elcoro, J. Cano, M. G. Vergniory, Z. Wang, C. Felser, M. I. Aroyo, and B. A. Bernevig, Topological quantum chemistry, Nature (London) **547**, 298 (2017).

[19] E. Prodan, Robustness of the spin-Chern number, Phys. Rev. B **80**, 125327 (2009).

[20] K.-S. Lin, G. Palumbo, Z. Guo, Y. Hwang, J. Blackburn, D. P. Shoemaker, F. Mahmood, Z. Wang, G. A. Fiete, B. J. Wieder, and B. Bradlyn, Spin-resolved topology and partial axion angles in three-dimensional insulators, Nat. Commun. **15**, 550 (2024).

[21] G. F. Lange, A. Bouhon, and R.-J. Slager, Spin texture as a bulk indicator of fragile topology, Phys. Rev. Res. **5**, 033013 (2023).

[22] T. Fu, R.-Y. Zhang, S. Jia, C. T. Chan, and S. Wang, Near-field spin Chern number quantized by real-space topology of optical structures, Phys. Rev. Lett. **132**, 233801 (2024).

[23] R. González-Hernández and B. Uribe, Spin Weyl topological insulators, Phys. Rev. B **109**, 045126 (2024).

[24] M. Asorey, Space, matter and topology, Nat. Phys. **12**, 616 (2016).

[25] A. M. Essin, J. E. Moore, and D. Vanderbilt, Magnetoelectric polarizability and axion electrodynamics in crystalline insulators, Phys. Rev. Lett. **102**, 146805 (2009).

[26] N. Varnava and D. Vanderbilt, Surfaces of axion insulators, Phys. Rev. B **98**, 245117 (2018).

[27] R. Moessner and J. E. Moore, *Topological Phases of Matter* (Cambridge University Press, Cambridge, 2021)

[28] L. Fu and C. L. Kane, Time reversal polarization and a Z_2 adiabatic spin pump, Phys. Rev. B **74**, 195312 (2006).

[29] L. Fu, C. L. Kane, and E. J. Mele, Topological insulators in three dimensions, Phys. Rev. Lett. **98**, 106803 (2007).

[30] Y. Yang, Z. Xu, L. Sheng, B. Wang, D. Y. Xing, and D. N. Sheng, Time-reversal-symmetry-broken quantum spin Hall effect, Phys. Rev. Lett. **107**, 066602 (2011).

[31] J. Qiao, J. Zhou, Z. Yuan, and W. Zhao, Calculation of intrinsic spin Hall conductivity by wannier interpolation, Phys. Rev. B **98**, 214402 (2018).

[32] Y. Bai, L. Cai, N. Mao, R. Li, Y. Dai, B. Huang, and C. Niu, Doubled quantum spin Hall effect with high-spin Chern number in α-antimonene and α-bismuthene, Phys. Rev. B **105**, 195142 (2022).

[33] M. König, S. Wiedmann, C. Brüne, A. Roth, H. Buhmann, L. W. Molenkamp, X.-L. Qi, and S.-C. Zhang, Quantum spin Hall insulator state in HgTe quantum wells, Science **318**, 766 (2007).

[34] Y. Xue, W. Xu, B. Zhao, J. Zhang, and Z. Yang, Antiferromagnetic quantum spin Hall insulators with high spin Chern numbers, Phys. Rev. B **108**, 075138 (2023).

[35] N. Shumiya, M. S. Hossain, J.-X. Yin, Z. Wang, M. Litskevich, C. Yoon, Y. Li, Y. Yang, Y.-X. Jiang, G. Cheng, Y.-C. Lin, Q. Zhang, Z.-J. Cheng, T. A. Cochran, D. Multer, X. P. Yang, B. Casas, T.-R. Chang, T. Neupert, Z. Yuan *et al.*, Evidence of a room-temperature quantum spin Hall edge state in a higher-order topological insulator, Nat. Mater. **21**, 1111 (2022).

[36] Y.-T. Yao, X. Zhou, Y.-C. Hung, H. Lin, A. Bansil, and T.-R. Chang, Feature-energy duality of topological boundary states in a multilayer quantum spin Hall insulator, Phys. Rev. B **109**, 155143 (2024).

[37] C.-H. Hsu, X. Zhou, Q. Ma, N. Gedik, A. Bansil, V. M. Pereira, H. Lin, L. Fu, S.-Y. Xu, and T.-R. Chang, Purely rotational symmetry-protected topological crystalline insulator $\alpha-Bi_4Br_4$, 2D Mater. **6**, 031004 (2019).

[38] F. Tang, H. C. Po, A. Vishwanath, and X. Wan, Efficient topological materials discovery using symmetry indicators, Nat. Phys. **15**, 470 (2019).

[39] Y. Sun, Y. Zhang, C. Felser, and B. Yan, Strong intrinsic spin Hall effect in the TaAs family of Weyl semimetals, Phys. Rev. Lett. **117**, 146403 (2016).

[40] A. A. Burkov, Anomalous Hall effect in Weyl metals, Phys. Rev. Lett. **113**, 187202 (2014).

[41] Z. Fang, N. Nagaosa, K. S. Takahashi, A. Asamitsu, R. Mathieu, T. Ogasawara, H. Yamada, M. Kawasaki, Y. Tokura, and K. Terakura, The anomalous Hall effect and magnetic monopoles in momentum space, Science **302**, 92 (2003).

[42] L. Elcoro, B. J. Wieder, Z. Song, Y. Xu, B. Bradlyn, and B. A. Bernevig, Magnetic topological quantum chemistry, Nat. Commun. **12**, 5965 (2021).

[43] S. Tian, S. Gao, S. Nie, Y. Qian, C. Gong, Y. Fu, H. Li, W. Fan, P. Zhang, T. Kondo, S. Shin, J. Adell, H. Fedderwitz, H. Ding, Z. Wang, T. Qian, and H. Lei, Magnetic topological insulator $MnBi_6Te_{10}$ with a zero-field ferromagnetic state and gapped Dirac surface states, Phys. Rev. B **102**, 035144 (2020).

[44] A. Jain, S. P. Ong, G. Hautier, W. Chen, W. D. Richards, S. Dacek, S. Cholia, D. Gunter, D. Skinner, G. Ceder, and K. A. Persson, Commentary: The materials project: A materials genome approach to accelerating materials innovation, APL Mater. **1**, 011002 (2013).

[45] G. Kresse and J. Furthmüller, Efficient iterative schemes for *ab initio* total-energy calculations using a plane-wave basis set, Phys. Rev. B **54**, 11169 (1996).

[46] A. A. Mostofi, J. R. Yates, G. Pizzi, Y.-S. Lee, I. Souza, D. Vanderbilt, and N. Marzari, An updated version of wannier90: A tool for obtaining maximally-localised wannier functions, Comput. Phys. Commun. **185**, 2309 (2014).

[47] Python tight binding open-source package, https://www.physics.rutgers.edu/pythtb/.

[48] A. C. Tyner, Berryeasy: a GPU enabled python package for diagnosis of nth-order and spin-resolved topology in the presence of fields and effects, J. Phys.: Condens. Matter **36**, 325902 (2024).

[49] H. Zhang, C.-X. Liu, X.-L. Qi, X. Dai, Z. Fang, and S.-C. Zhang, Topological insulators in Bi_2Se_3, Bi_2Te_3 and Sb_2Te_3 with a single Dirac cone on the surface, Nat. Phys. **5**, 438 (2009).

[50] H. Wang, D. Wang, Z. Yang, M. Shi, J. Ruan, D. Xing, J. Wang, and H. Zhang, Dynamical axion state with hidden pseudospin chern numbers in $MnBi_2Te_4$-based heterostructures, Phys. Rev. B **101**, 081109(R) (2020).